 CMES, vol.73, no.1, pp.1-22, 2011

An Overrange Collocation Method

Y.-M. Guo[1]

Abstract: In this paper, a new meshless method called the overrange collocation method (ORCM) is proposed. By introducing some collocation points, which are located at outside of domain of the analyzed body, unsatisfactory issue of the positivity conditions of boundary points in collocation methods can be avoided. Because the overrange points are used only in interpolating calculation, no over-constrained condition is imposed into the solved boundary value problems. Poisson's problem and the linear elastic cantilever beam problem are analyzed by using the ORCM.

Keywords: Meshless method, collocation method, overrange points, moving least-square approximation, positivity conditions.

1 Introduction

Many meshless methods have been proposed. The early representatives of meshless methods are the diffuse element method [Nayroles, Touzot, Villon (1992)], the element free Galerkin method [Belytschko, Lu, Gu (1994)], the reproducing kernel particle method [Liu et al. (1995)], the finite point method [Onate et al. (1996a)], the hp-clouds method [Duarte, Oden (1996)], the partition of unity method [Melenk, Babuska (1996)], the meshless local Petrov-Galerkin (MLPG) approach [Atluri, Zhu (1998)], the local boundary integral equation method [Zhu, Zhang, Atluri (1998)], and the point collocation method (PCM) based on reproducing kernel approximations [Aluru (2000)]. Some meshless methods are based on weak form, in which background meshes are inevitable in implementation to obtain the numerical integration. Some meshless methods are truly meshless methods, in which no background mesh is introduced. In most meshless techniques, however, complicated non-polynomial interpolation functions are used which render the integration of the weak form rather difficult. Failure to perform the integration accurately results in loss of accuracy and possibly stability of solution scheme. The integration of complicated non-polynomial interpolation function also costs much CPU time.

[1] Kagoshima University, Kagoshima City, Japan

The collocation method is a kind of truly meshless method, and has no issues of the integration scheme, the integration accuracy and the integration CPU time. Several collocation methods based on different types of approximations or interpolations have been proposed in the literature. Onate et al. [Onate et al. (1996a)] have proposed a finite point method based on weighted least squares interpolations for the analyses of convective transport and fluid flow problems. Onate et al. [Onate et al. (1996b)] have also proposed a residual stabilization procedure, adequate for the finite point method, and further extended the finite point method to the solution of the advective-convective transport equations as well as those governing the flow of compressible fluids. Boroomand, Tabatabaei and Onate [Boroomand, Tabatabaei, Onate (2005)] have presented a stabilized version of the finite point method to eliminate the ill-conditioning effect due to directional arrangement of the points. Aluru [Aluru (2000)] has presented a point collocation method based on reproducing kernel approximations for numerical solution partial differential equations with appropriate boundary conditions. Jin, Li and Aluru [Jin, Li, Aluru (2004)] have shown the robustness of collocation meshless methods can be improved by ensuring that the positivity conditions are satisfied when constructing approximation functions and their derivatives. Atluri, Liu and Han [Atluri, Liu, Han (2006a)] have presented a MLPG mixed collocation method by using the Dirac delta function as the test function in the MLPG method, and shown that the MPLG mixed collocation method is more efficient than the other MLPG implementations, including the MLPG finite volume method. Atluri, Liu and Han [Atluri, Liu, Han (2006b)] have proposed a finite difference method, within the framework of the MLPG approach, for solving solid mechanics problems. Wu, Shen and Tao [Wu, Shen, Tao (2007)] have used the MLPG collocation method to compute two-dimensional heat conduction problems in irregular domain. Li and Atluri [Li, Atluri (2008a)] have demonstrated the suitability and versatility of the MLPG mixed collocation method by solving the problem of topology-optimization of elastic structures. In addition, the MLPG mixed collocation method has also been successfully used in material orientation and topology optimization of anisotropic solids and structures [Li, Atluri (2008b)]. Chantasiriwan [Chantasiriwan (2006)] has provided results of using the multiquadric collocation method to solve the lid-driven cavity flow problem. Wen and Hon [Wen, Hon (2007)] have performed a geometrically nonlinear analysis of Reissner-Mindlin plate by using a meshless collocation method based on the smooth radial basis functions. Kosec and Sarler [Kosec, Sarler (2008)] have explored the application of the mesh-free local radial basis function collocation method in solution of coupled heat transfer and fluid flow problems in Darcy porous media. Wu, Chiu and Wang [Wu, Chiu, Wang (2008)] have developed a mesh-free collocation method based on differential reproducing kernel approximations for the three-dimensional analysis of simply-supported, doubly curved

functionally graded magneto-electro-elastic shells under the mechanical load, electric displacement and magnetic flux. Yang et al. [Yang et al. (2008)] have introduced a computational procedure based on meshless generalized finite difference method and serial magnetic resonance imaging data to quantify patient-specific carotid atherosclerotic plaque growth functions and simulate plaque progression.

While, the robustness of the collocation methods is an issue especially in which scattered and random points are used. To improve the robustness of the collocation methods, Nayroles, Touzot and Villon [Nayroles, Touzot, Villon (1992)] suggested that the positivity conditions could be important when using the collocation methods. Jin, Li and Aluru [Jin, Li, Aluru (2004)] have proposed techniques, based on modification of weighting functions, to ensure satisfaction of positivity conditions when using a scattered set of points. For boundary points, however, the positivity conditions cannot be satisfied, obviously, so that it is possible to get large numerical errors from the boundary points when using the collocation methods. Guo [Guo (2009)] has proposed a hybrid PCM/FEM, by introducing a boundary layer of finite element in boundary domain of body, unsatisfactory issue of the positivity conditions of boundary points can be avoided, and the complicated boundary conditions can be easily imposed with the boundary layer of finite element.

In this paper, a new meshless method called the overrange collocation method (ORCM) is proposed. By introducing some collocation points, which are located at outside of domain of the analyzed body, unsatisfactory issue of the positivity conditions of boundary points in collocation methods can be avoided. Because the overrange points are used only in interpolating calculation, no over-constrained condition is imposed into the solved boundary value problems. The ORCM does not demand any specific kind of partial differential equation, therefore it shows promise of wide engineering applications of the ORCM. Poisson's problem and the linear elastic cantilever beam problem are analyzed by using the ORCM.

This paper is organized as follows. In Section 2, collocation scheme of the ORCM is described, in which overrange points are introduced. In Section 3, a modified MLS approximation is developed, whose shape functions have Kronecker-delta property. In Section 4, a local coordinate system is introduced, which rends formulas of the shape function derivatives very simple. In Section 5, the positivity conditions are described. In Section 6, Poisson's equation and the linear elastic cantilever beam problem are tested, and their numerical solutions are compared with the exact solutions to illustrate the implementation and convergence of the ORCM. In Section 7, conclusions are drawn.

2 Collocation Scheme

Let us assume a scalar problem governed by a partial differential equation:

$$D(u) = b, \ in \ \Omega \tag{1}$$

with boundary conditions

$$T(u) = t, \ on \ \Gamma_t \tag{2}$$

$$u - u_c = 0, \ on \ \Gamma_u \tag{3}$$

to be satisfied in a domain Ω with boundary $\Gamma = \Gamma_t \cup \Gamma_u$, where D and T are appropriate differential operators, u is the problem unknown function, b and t are external forces or sources acting over Ω and along Γ_t, respectively. u_c is the assigned value of u over Γ_u.

Consider taking some collocation points in Ω, at which Eq. 1 is satisfied, and some collocation points on Γ_t, at which both Eq. 1 and Eq.2 are satisfied, as well as some collocation points on Γ_u, at which both Eq.1 and Eq.3 are satisfied. Besides the collocation points over Ω, let us assume other collocation points located at outside of Ω and call them overrange points (see Fig. 1), at which no satisfaction of any governing partial differential equation or boundary condition is needed. Therefore, no over-constrained condition is imposed into the boundary value problem. While the overrange points can be used in interpolating calculation of boundary points, so that the unsatisfactory issue of the positivity conditions of boundary points in collocation methods can be avoided.

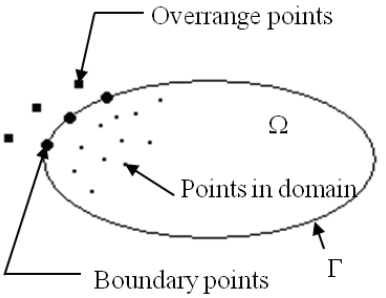

Figure 1: Overrange points, boundary points and points in domain

Let us assume that the number of points in domain is $\mathrm{K_d}$, the number of boundary points is $\mathrm{K_b}$ and the number of overrange points is $\mathrm{K_o}$, then the number of unknown variables is $2(\mathrm{K_d}+\mathrm{K_b}+\mathrm{K_o})$ for a 2-D problem. Because the number of equations of the ORCM is $2(K_d+K_b)+2K_b$, by taking the same number of the equations with that of the unknown variables, we obtain that the number of the overrange points $\mathrm{K_o}$ must be equal to the number of boundary points $\mathrm{K_b}$.

3 The MLS approximation with Kronecker-delta property

In the classical moving least-square (MLS) approximation, the shape functions have no Kronecker-delta property, so that the essential node condition cannot be imposed on boundaries. In this paper, a modified MLS approximation is used, its shape functions have Kronecker-delta property. Therefore, the unsatisfactory issue of the essential node condition can be avoided in the modified MLS approximation.

Consider a small domain Ω_x, the neighborhood of a point x_1, which is located in Ω or on Γ. Over Ω_x, u can be approximated by the MLS approximation. The MLS approximation with quadratic basis is not sensitive to the number of nodes in a sub-domain [Onate et al. (1996a)]. Derivatives of interpolations using the MLS approximation show smaller oscillations than those in the partition of unity method, [Atluri, Kim, Cho (1999)].

Over a number of randomly located nodes $\{x_i\}$, $i=1,\ 2,\ \cdots,\ n$, the MLS approximation u^h of u can be defined by

$$u^h = \mathbf{p}^T(\mathbf{x})\ \boldsymbol{\alpha},\ \forall \mathbf{x} \in \Omega_x \tag{4}$$

where $\mathbf{p}^T(\mathbf{x}) = [p_1(\mathbf{x})\ p_2(\mathbf{x})\ \cdots\ p_m(\mathbf{x})]$ is a complete monomial basis of order m which is a function of the space coordinates $\mathbf{x} = [\mathrm{x\ y\ z}]^{\mathrm{T}}$. $\boldsymbol{\alpha}$ is a vector of unknown polynomial coefficients.

$$\boldsymbol{\alpha} = \begin{bmatrix}\alpha_1 & \alpha_2 & \cdots & \alpha_m\end{bmatrix}^T \tag{5}$$

For example, for a 2-D problem,

$$\mathbf{p}^T(\mathbf{x}) = \begin{bmatrix}1\ x\ y\ x^2\ xy\ y^2\end{bmatrix} \tag{6}$$

this is a quadratic basis, and m=6.

A weighted least-square solution is obtained for $\boldsymbol{\alpha}$ from the following system of n equations in m unknown (n is larger than m):

$$\mathbf{u}^h = \mathbf{H}\,\boldsymbol{\alpha} \tag{7}$$

where

$$\mathbf{u}^h = \begin{bmatrix} u_1^h & u_2^h & \cdots & u_n^h \end{bmatrix}^T \tag{8}$$

is a vector of the nodal MLS approximation of function u, and

$$\mathbf{H} = \begin{bmatrix} \mathbf{p}^T(\mathbf{x}_1) \\ \mathbf{p}^T(\mathbf{x}_2) \\ \vdots \\ \mathbf{p}^T(\mathbf{x}_n) \end{bmatrix}_{n \times m} \tag{9}$$

The classical least-square solution of the above over-constrained system does not guarantee exact satisfaction of any of the equations of Eq. 7. Non-satisfaction of the first equation would then mean $u_1^h \neq \mathbf{p}^T(\mathbf{x}_1)\ \boldsymbol{\alpha}$, which, in turn, means that the least-square interpolation at node 1 is not equal to value of the node. Hence, a different approach to weighted least-squares solution can be adopted: Out of the n equations of Eq. 7, let the first equation (corresponding to node 1) be satisfied exactly and the rest in the least-square sense. This is done by using the first equation to eliminate α_1 from the rest of equations:

$$\alpha_1 = u_1^h - (\alpha_2 x_1 + \alpha_3 y_1 + \alpha_4 x_1^2 + \alpha_5 x_1 y_1 + \alpha_6 y_1^2) \tag{10}$$

Substituting for α_1 in Eq. 7, the reduced system of equations can be obtained:

$$\bar{\mathbf{u}}^h = \bar{\mathbf{H}}\ \bar{\boldsymbol{\alpha}} \tag{11}$$

where

$$\bar{\mathbf{u}}^h = \begin{bmatrix} u_2^h - u_1^h & u_3^h - u_1^h & \cdots & u_n^h - u_1^h \end{bmatrix}^T \tag{12}$$

$$\bar{\mathbf{H}} = \begin{bmatrix} x_2 - x_1 & y_2 - y_1 & x_2^2 - x_1^2 & x_2 y_2 - x_1 y_1 & y_2^2 - y_1^2 \\ x_3 - x_1 & y_3 - y_1 & x_3^2 - x_1^2 & x_3 y_3 - x_1 y_1 & y_3^2 - y_1^2 \\ \vdots & \vdots & \vdots & \vdots & \vdots \\ x_n - x_1 & y_n - y_1 & x_n^2 - x_1^2 & x_n y_n - x_1 y_1 & y_n^2 - y_1^2 \end{bmatrix} = \begin{bmatrix} \bar{\mathbf{p}}^T(\mathbf{x}_2) \\ \bar{\mathbf{p}}^T(\mathbf{x}_3) \\ \vdots \\ \bar{\mathbf{p}}^T(\mathbf{x}_n) \end{bmatrix} \tag{13}$$

$$\bar{\boldsymbol{\alpha}} = \begin{bmatrix} \alpha_2 & \alpha_3 & \cdots & \alpha_m \end{bmatrix}^T \tag{14}$$

The coefficient vector $\bar{\boldsymbol{\alpha}}$ is determined by minimizing a weighted discrete L_2 norm, defined as:

$$J = \sum_{i=2}^{n} w(\mathbf{x}_i)\ \left[\bar{\mathbf{p}}^T(\mathbf{x}_i)\ \bar{\alpha} - \bar{u}_i\right]^2 = \left[\bar{\mathbf{H}}\ \bar{\boldsymbol{\alpha}} - \bar{\mathbf{u}}\right]^T \mathbf{W}\ \left[\bar{\mathbf{H}}\ \bar{\boldsymbol{\alpha}} - \bar{\mathbf{u}}\right] \tag{15}$$

where $w(\mathbf{x})$ is the weight function, with $w(\mathbf{x})>0$ for all nodes in the support of $w(\mathbf{x})$ (the support is considered to be equal to Ω_x in this paper), $\mathbf{x}_i$ denotes the value of $\mathbf{x}$ at node i, and the matrices $\mathbf{W}$ is defined as

$$\mathbf{W} = \begin{bmatrix} w(\mathbf{x}_2) & 0 & \cdots & 0 \\ 0 & w(\mathbf{x}_3) & \cdots & 0 \\ \cdots & \cdots & \cdots & \cdots \\ 0 & 0 & \cdots & w(\mathbf{x}_n) \end{bmatrix}_{(n-1)\times(n-1)} \tag{16}$$

$$\bar{u}_i = \hat{u}_i - \hat{u}_1,\ i = 2,\ 3,\ \cdots,\ n \tag{17}$$

and

$$\bar{\mathbf{u}} = [\hat{u}_2 - \hat{u}_1\ \hat{u}_3 \text{ - } \hat{u}_1\ \cdots\ \hat{u}_n - \hat{u}_1]^T \tag{18}$$

where $\hat{u}_i,\ i = 1,\ 2,\ \cdots,\ n$ are the fictitious nodal values of the function u.
Minimizing J in Eq. 15 with respect to $\bar{\boldsymbol{\alpha}}$ yields

$$\bar{\boldsymbol{\alpha}} = \mathbf{A}^{-1}\ \mathbf{B}\ \bar{\mathbf{u}} \tag{19}$$

where

$$\mathbf{B} = \bar{\mathbf{H}}^T \mathbf{W} \tag{20}$$

$$\mathbf{A} = \mathbf{B}\ \bar{\mathbf{H}} \tag{21}$$

Substituting Eq. 19 into Eq. 11 gives a relation which may be written as the form of an interpolation function, as

$$\bar{\mathbf{u}}^h = \bar{\mathbf{H}}\ \mathbf{A}^{-1}\ \mathbf{B}\bar{\mathbf{u}} \tag{22}$$

Eq. 10 can be rewritten as:

$$\alpha_1 = u_1^h - \mathbf{s}(\mathbf{x}_1)\,\bar{\alpha} \tag{23}$$

where

$$\mathbf{s}(\mathbf{x}_1) = \begin{bmatrix} x_1 & y_1 & {x_1}^2 & x_1 y_1 & y_1^2 \end{bmatrix} \tag{24}$$

Eq. 4 can be written as:

$$u^h = \alpha_1 + \mathbf{s}(\mathbf{x})\ \bar{\alpha} \tag{25}$$

where

$$\mathbf{s}(\mathbf{x}) = \begin{bmatrix} x & y & x^2 & xy & y^2 \end{bmatrix} \tag{26}$$

Substituting Eq. 19 and Eq. 23 into Eq. 25, the following equation can be obtained:

$$u^h = u_1^h + \mathbf{q}(\mathbf{x})\ \mathbf{A}^{-1}\mathbf{B}\bar{\mathbf{u}} \tag{27}$$

where

$$\mathbf{q}(\mathbf{x}) = \mathbf{s}(\mathbf{x})\ -\mathbf{s}(\mathbf{x}_1) \tag{28}$$

$$\because\ \mathbf{q}(\mathbf{x}_1) = 0 \tag{29}$$

$$\therefore\ u^h(\mathbf{x}_1) = u_1^h \tag{30}$$

$\hat{\mathbf{u}}$ may be defined as:

$$\hat{\mathbf{u}} = [\hat{u}_1\ \hat{u}_2\ \cdots\ \hat{u}_n]^T \tag{31}$$

then, from Eq. 27, the following equation may be obtained:

$$u^h = \mathbf{N}(\mathbf{x})\,\hat{\mathbf{u}} \tag{32}$$

where

$$\underset{1\times n}{\mathbf{N}(\mathbf{x})} = \left[1 - \left(\underset{1\times(\mathrm{m}-1)}{\mathbf{q}(\mathbf{x})}\ \underset{(\mathrm{m}-1)\times(m-1)}{\mathbf{A}^{-1}}\ \underset{(\mathrm{m}-1)\times(n-1)}{\mathbf{B}}\ \underset{(\mathrm{n}-1)\times 1}{\mathbf{1}}\right) \vdots\right.$$

$$\left.\underset{1\times(\mathrm{m}-1)}{\mathbf{q}(\mathbf{x})}\ \underset{(\mathrm{m}-1)\times(m-1)}{\mathbf{A}^{-1}}\ \underset{(\mathrm{m}-1)\times(n-1)}{\mathbf{B}}\right] \tag{33}$$

In Eq. 33, **1** is vector of dimension (n-1) with all entries being equal to unity.

Recall form Eq. 29, using this result in Eq. 33, the Kronecker-delta property of $\mathbf{N}(\mathbf{x})$ may be established:

$$\underset{1\times n}{\mathbf{N}(\mathbf{x}_1)} = \begin{bmatrix} 1 & 0 & 0 & \cdots & 0 \end{bmatrix} \tag{34}$$

It means that at node 1, the shape function for node 1 takes a value of unity and all other shape function take zero values. Therefore, Eq. 33 is the shape functions of the MLS approximation with Kronecker-delta property.

From Eq. 32 and Eq. 30, the following result can be obtained:

$$\hat{u}_1 = u^h(\mathbf{x}_1) = u_1^h \tag{35}$$

In this paper, the weight functions $w(\mathbf{x})$ may use a spline function as follows:

$$w(\mathbf{x}) = 1 - 6\left(\frac{d}{r}\right)^2 + 8\left(\frac{d}{r}\right)^3 - 3\left(\frac{d}{r}\right)^4,\ 0 \le d \le r \tag{36a}$$

$$w(\mathbf{x}) = 0,\ d \ge r \tag{36b}$$

where $d = |\mathbf{x} - \mathbf{x}_1|$ is the distance from point x to the center node x_1, and r is the radius of Ω_x, which is taken as a circle for a 2-D problem and its center is the point x_1.

4 The local coordinate system

As anisotropy of the point distribution in Ω_x, matrix $\mathbf{A}$ in Eq. 21 becomes ill-conditioned and the quality of the approximation deteriorates. In order to prevent such undesirable effect, a local coordinate system $\xi,\ \eta$ is chosen with origin at the node x_1 for a 2-D problem, see [Boroomand, Tabatabaei, Onate (2005)],

$$\xi = \frac{x - x_1}{R_x} \tag{37a}$$

$$\eta = \frac{y - y_1}{R_y} \tag{37b}$$

where R_x and R_y denote maximum distances along x and y measured from the point x_1 to exterior nodes in Ω_x. In Eq. 36a, the spline function has now the following form in terms of the local coordinates:

$$w(\boldsymbol{\xi}) = 1 - 6\left(\frac{\xi^2 + \eta^2}{\rho^2}\right) + 8\left(\frac{\xi^2 + \eta^2}{\rho^2}\right)^{\frac{3}{2}} - 3\left(\frac{\xi^2 + \eta^2}{\rho^2}\right)^2 \tag{38}$$

$\rho = 6$ is used in this paper and as usual $-1 \le \xi \le 1,\ -1 \le \eta \le 1$.

The matrix $\mathbf{A}$ is not longer dependent on the dimensions of Ω_x. The approximate function is also expressed in terms of the local coordinates as

$$u^h(\boldsymbol{\xi}) = \mathbf{N}(\boldsymbol{\xi})\hat{\mathbf{u}} \tag{39}$$

$\mathbf{A}^{-1}\mathbf{B}$ in Eq. 33 can be defined as $\mathbf{C}$:

$$\mathbf{C} = \mathbf{A}^{-1}\mathbf{B} \tag{40}$$

Then, from Eq. 33, entries of $\mathbf{N}(\mathbf{x})$ for the quadratic basis (m=6) can be written as:

$$N_1(\mathbf{x}) = 1 - \left[(x-x_1)\sum_{i=1}^{n-1} C_{1i} + (y-y_1)\sum_{i=1}^{n-1} C_{2i} + \left(x^2-x_1^2\right)\sum_{i=1}^{n-1} C_{3i} + (xy-x_1y_1)\sum_{i=1}^{n-1} C_{4i} + \left(y^2-y_1^2\right)\sum_{i=1}^{n-1} C_{5i} \right] \quad (41)$$

$$N_{i+1}(\mathbf{x}) = (x-x_1)C_{1i} + (y-y_1)C_{2i} + \left(x^2-x_1^2\right)C_{3i} + (xy-x_1y_1)C_{4i} + \left(y^2-y_1^2\right)C_{5i} \ (i=1,\ 2,\ \cdots,\ n-1) \quad (42)$$

where $C_{ji},\ (j=1,\ 2,\ \cdots,\ 5;\ i=1,\ 2,\ \cdots,\ n-1)$ are entries of $\mathbf{C}$.

At the point x_1, because $\xi_1 = 0,\ \eta_1 = 0$, then the first-order derivatives of the shape function with the local coordinates can be obtained from Eqs. 41 and 42:

$$\frac{\partial \mathbf{N}(\boldsymbol{\xi}_1)}{\partial \xi} = \left[-\sum_{i=1}^{n-1} C_{1i} \quad C_{11} \quad C_{12} \quad \cdots \quad C_{1(n-1)} \right] \quad (43)$$

$$\frac{\partial \mathbf{N}(\boldsymbol{\xi}_1)}{\partial \eta} = \left[-\sum_{i=1}^{n-1} C_{2i} \quad C_{21} \quad C_{22} \quad \cdots \quad C_{2(n-1)} \right] \quad (44)$$

From Eqs. 43 and 44, we may see that formulas of the shape function derivatives with the local coordinates are very simple, and in fact, it is a merit of the ORCM using the local coordinates.

5 The positivity conditions

The positivity conditions on the approximation function $N_i(\mathbf{x})$ of Eq. 33 and its second-order derivatives are stated as [Jin, Li, Aluru (2004)],

$$N_i(\mathbf{x}_j) \geq 0 \quad (45)$$

$$\nabla^2 N_i(\mathbf{x}_j) \geq 0,\ j \neq i \quad (46)$$

$$\nabla^2 N_i(\mathbf{x}_i) < 0 \quad (47)$$

where $N_i(\mathbf{x}_j)$ is the approximation function of a point i evaluated at a point j.

Patankar [Patankar (1980)] included the positivity conditions in a series of basic rules for the construction of finite differences and pointed out that the consequence of violating the positivity conditions give a physically unrealistic solution. It has

been shown that the satisfaction of the positivity conditions ensures the convergence of the finite difference method with arbitrary irregular meshes for some class of elliptic problems [Demkowicz, Karafilt, Liszka (1984)]. It has been shown that the significance of the positivity conditions in meshless collocation approaches, and violation of the positivity conditions can significantly result in a large error in the numerical solution [Jin, Li, Aluru (2004)].

For a point x_1 on Γ, if no overrange point is used in its Ω_x, the positivity conditions on the boundary point cannot be satisfied, obviously. But by introducing some overrange points of Ω in the Ω_x, the unsatisfactory issue of the positivity conditions of the boundary point can be avoided in the ORCM.

6 Numerical examples

6.1 Poisson's equation

Firstly, Poisson's equation is analyzed by using the ORCM, and their numerical solutions are compared with the exact solutions to illustrate the implementation and convergence of the present ORCM.

For the purpose of error estimation and convergence studies, the Sobolev norm $\|u\|_0$, and the norm of the first-order derivative vector of u, $\|\mathbf{q}\|_0$ are calculated. These norms are defined as

$$\|u\|_0 = \left(\int_\Omega u^2 d\Omega \right)^{1/2} \tag{48}$$

$$\|\mathbf{q}\|_0 = \left(\int_\Omega \mathbf{q}^{\mathrm{T}} \cdot \mathbf{q} \, d\Omega \right)^{1/2} \tag{49}$$

where

$$\mathbf{q} = \begin{bmatrix} \partial u/\partial x & \partial u/\partial y \end{bmatrix}^{\mathrm{T}} = \begin{bmatrix} q_x & q_y \end{bmatrix}^{\mathrm{T}} \tag{50}$$

The relative errors for $\|u\|_0$ and $\|\mathbf{q}\|_0$ are defined as

$$R_0 = \frac{\|u^{num} - u^{exa}\|_0}{\|u^{exa}\|_0} \tag{51}$$

$$R_q = \frac{\|\mathbf{q}^{num} - \mathbf{q}^{exa}\|_0}{\|\mathbf{q}^{exa}\|_0} \tag{52}$$

The results from the ORCM are studied for the Poisson's equation with a given source function $p = (x+y)/10$ in the 1×1 domain, for which the exact solution is taken to be

$$u = -\frac{1}{12}\left(x^3+y^3\right) + \frac{3}{10}\left(x^2y+xy^2\right) \tag{53}$$

A Dirichlet problem is solved, for which the essential boundary condition is imposed on all sides, and two mixed problem, the first mixed problem (the essential boundary condition is imposed on left and right sides and the flux boundary condition is prescribed on top and bottom sides of the domain) and the second mixed problem (the essential boundary condition is imposed on top and bottom sides and the flux boundary condition is prescribed on left and right sides of the domain), are solved, too.

Regular nodal models of $89(9\times 9+8)$ ($K_d = 5\times 5,\ K_b = K_o = 32$) nodes, $129(11\times 11+8)$ ($K_d = 7\times 7,\ K_b = K_o = 40$) nodes and $177(13\times 13+8)$ ($K_d = 9\times 9,\ K_b = K_o = 48$) nodes are used to study the convergence with nodal model refinement of the ORCM. Overrange points of one layer, which are located at outside of the four sides of the domain, are used. To meet the condition of $\mathrm{K_b} = \mathrm{K_o}$, 8 nodes are added to the boundary points, which are located on the boundary near the four corners of the domain, for all the three nodal models.

The results of relative errors and convergence are shown in Fig. 2 for the first mixed problem. This figure shows that the ORCM works quite well.

Figs. 3, 4 and 5 show values of u of Poisson's equation at x=0.5 by regular nodal model of 89 nodes, for Dirichlet problem, the first mixed problem and the second mixed problem, respectively. Figs. 6, 7 and 8 show values of $\partial u/\partial x$ of Poisson' equation at x=0.5 by regular nodal model of 89 nodes, for Dirichlet problem, the first mixed problem and the second mixed problem, respectively. Figs. 9, 10 and 11 show values of $\partial u/\partial y$ of Poisson' equation at x=0.5 by regular nodal model of 89 nodes, for Dirichlet problem, the first mixed problem and the second mixed problem, respectively. It can be seen that some accurate results for the unknown variable and its derivatives are obtained.

One irregular nodal model of 89 ($K_d = 25,\ K_b = K_o = 32$) nodes is used, too. Fig. 12 shows distribution of the nodes in domain and the boundary nodes of the irregular nodal model.

Figs. 13, 14 and 15 show values of u of Poisson's equation at x=0.5 by irregular nodal model of 89 nodes, for Dirichlet problem, the first mixed problem and the second mixed problem, respectively. It can be seen that some accurate results for the unknown variable and its derivatives are obtained by using the irregular nodal model, too.

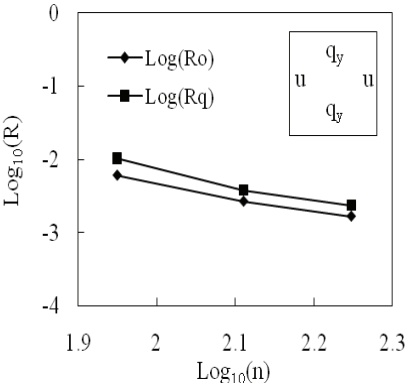

Figure 2: Relative errors and convergences for the first mixed problem of Poisson's equation (n is number of the nodes)

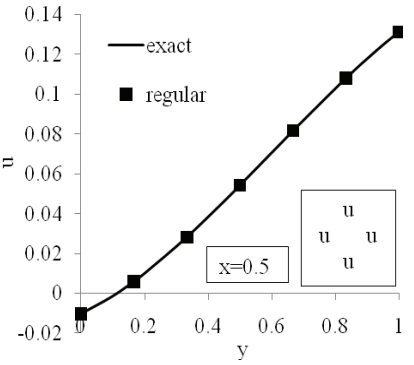

Figure 3: Values of u at x=0.5 by regular nodal model of 89 nodes, for Dirichlet problem of Poisson's equation

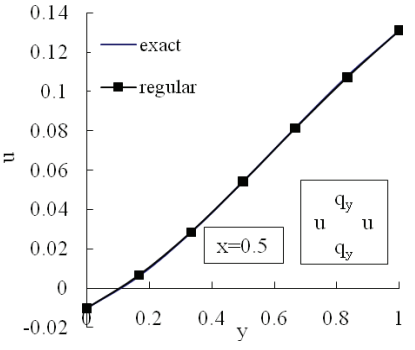

Figure 4: Values of u at x=0.5 by regular nodal model of 89 nodes, for the first mixed problem of Poisson's equation

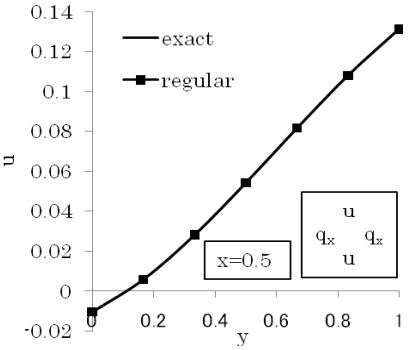

Figure 5: Values of u at x=0.5 by regular nodal model of 89 nodes, for the second mixed problem of Poisson's equation

6.2 The linear elastic cantilever beam problem

Secondly, the linear elastic cantilever beam problem is analyzed by using the ORCM, and their numerical solutions are compared with the exact solutions to illustrate the implementation and convergence of the ORCM.

The displacement and energy norms, $\|\mathbf{u}\|$ and $\|\varepsilon\|$ are calculated. These norms are

defined as

$$\|\mathbf{u}\| = \left(\int_{\Omega} \mathbf{u}^{\mathrm{T}} \cdot \mathbf{u} \, d\Omega \right)^{1/2} \tag{54}$$

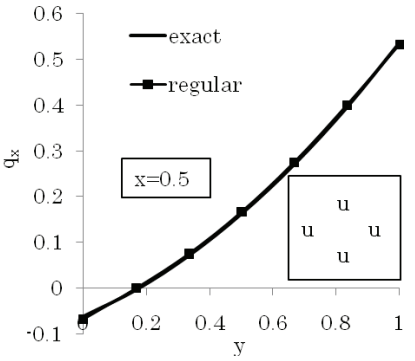

Figure 6: Values of $\partial u/\partial x$ at x=0.5 by regular nodal model of 89 nodes, for Dirichlet problem of Poisson's equation

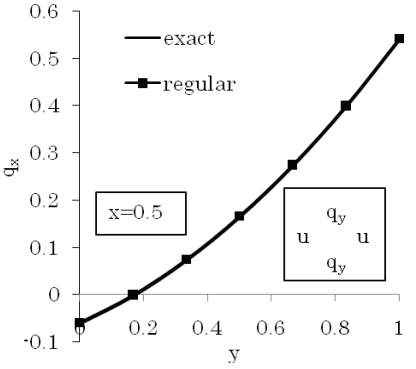

Figure 7: Values of $\partial u/\partial x$ at x=0.5 by regular nodal model of 89 nodes, for the first mixed problem of Poisson's equation

and

$$\|\varepsilon\| = \left(\frac{1}{2} \int_{\Omega} \sigma^{\mathrm{T}} \cdot \varepsilon \, d\Omega \right)^{1/2} \tag{55}$$

where$\mathbf{u} = \begin{bmatrix} u & v \end{bmatrix}^{\mathrm{T}}$ is the displacement vector, and $\varepsilon = \begin{bmatrix} \varepsilon_{11} & \varepsilon_{22} & \gamma_{12} \end{bmatrix}^{\mathrm{T}}$ and $\sigma = \begin{bmatrix} \sigma_{11} & \sigma_{22} & \sigma_{12} \end{bmatrix}^{\mathrm{T}}$ are the strain vector and stress vector, respectively.

The relative errors for $\|\mathbf{u}\|$ and $\|\varepsilon\|$ are defined as

$$R_u = \frac{\|\mathbf{u}^{num} - \mathbf{u}^{exa}\|}{\|\mathbf{u}^{exa}\|} \tag{56}$$

$$R_e = \frac{\|\varepsilon^{num} - \varepsilon^{exa}\|}{\|\varepsilon^{exa}\|} \tag{57}$$

The results from the ORCM are studied for the linear elastic cantilever beam problem (see Fig. 16), for which the following exact solution is given as

$$u = -\frac{P}{6EI}\left(y - \frac{D}{2}\right)\left[3x(2L-x) + (2+\nu)\,y(y-D)\right] \tag{58a}$$

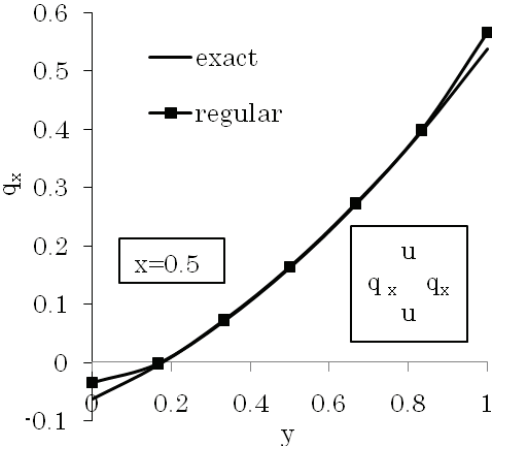

Figure 8: Values of $\partial u/\partial x$ at x=0.5 by regular nodal model of 89 nodes, for the second mixed problem of Poisson's equation

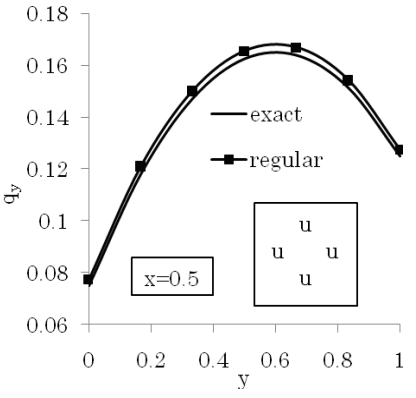

Figure 9: Values of $\partial u/\partial y$ at x=0.5 by regular nodal model of 89 nodes, for Dirichlet problem of Poisson's equation

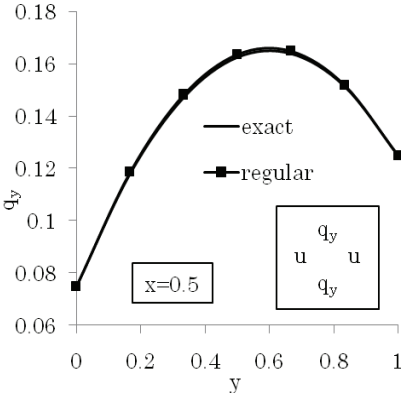

Figure 10: Values of $\partial u/\partial y$ at x=0.5 by regular nodal model of 89 nodes, for the first mixed problem of Poisson's equation

$$v = \frac{P}{6EI}\left[x^2(3L-x) + 3\nu(L-x)\left(y-\frac{D}{2}\right)^2 + \frac{4+5\nu}{4}D^2x\right] \tag{58b}$$

$$I = \frac{D^3}{12} \tag{59}$$

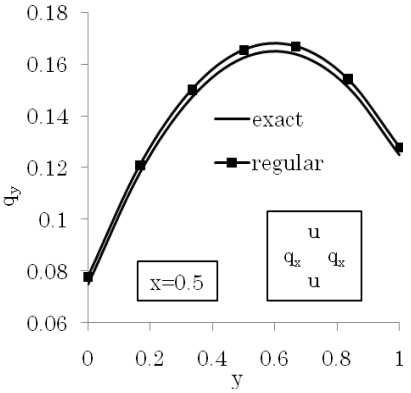

Figure 11: Values of $\partial u/\partial y$ at x=0.5 by regular nodal model of 89 nodes, for the second mixed problem of Poisson's equation

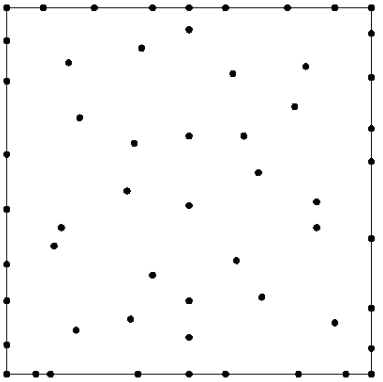

Figure 12: Irregularly distributed nodes in domain and boundary nodes used in Poisson's equation

The stress corresponding to Eqs. 58a and 58b are

$$\sigma_{11} = -\frac{P}{I}(L-x)\left(y-\frac{D}{2}\right) \tag{60a}$$

$$\sigma_{22} = 0 \tag{60b}$$

$$\sigma_{12} = -\frac{Py}{2I}(y-D) \tag{60c}$$

The problem is solved for the plane stress case with P=1, E=1, D=10, L=40. $\nu = 0.25$ is used. Boundary conditions of nodes on the left and the right boundaries (including the corner nodes) are chosen as:

$$u = u^{exa} \tag{61a}$$

$$v = v^{exa} \tag{61b}$$

Boundary conditions of nodes on the top and the bottom boundaries are chosen as:

$$\sigma_{12} = 0 \tag{62a}$$

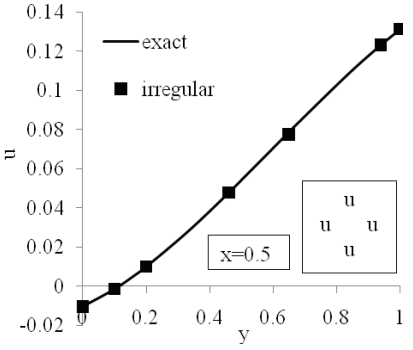

Figure 13: Values of u at x=0.5 by irregular nodal model of 89 nodes, for Dirichlet problem of Poisson's equation

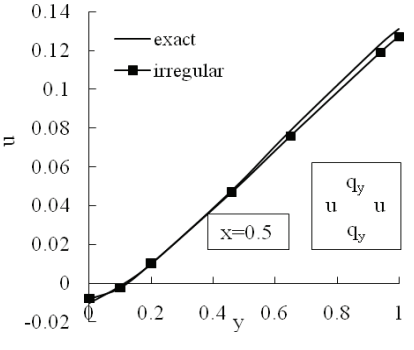

Figure 14: Values of u at x=0.5 by irregular nodal model of 89 nodes, for the first mixed problem of Poisson's equation

$$\sigma_{22} = 0 \tag{62b}$$

Regular nodal models of $53(9\times 5+8)(K_d = 5\times 1,\ K_b = K_o = 24)$nodes, $85(11\times 7+8)$ $(K_d = 7\times 3,\ K_b = K_o = 32)$ nodes and $125(13\times 9+8)$ $(K_d = 9\times 5,\ K_b = K_o = 40)$ nodes are used to study the convergence with nodal model refinement of the ORCM. Overrange points of one layer, which are located at outsides of boundary of the elastic cantilever beam, are used. To meet the condition of $K_b = K_o$, 8 nodes are added to the boundary points, which are located on the boundary near the four corners of the domain, for all the three nodal models.

The results of relative errors and convergence are shown in Fig. 17 for the linear elastic cantilever beam problem. This figure shows that the ORCM works quite well.

Fig. 18 shows values of u of the linear elastic cantilever beam problem at x=0.5L by regular nodal model of 125 nodes. Fig.19 shows values of v of the linear elastic cantilever beam problem at y=0.5D by regular nodal model of 125 nodes. Figs. 20 and 21 show values of $\sigma_{11}$and σ_{12}at x=0.5L by regular nodal model of 125 nodes, respectively. Figs. 22 and 23 show distributions of numerical displacement vectors (by the ORCM with regular nodal model of 125 nodes) and exact displacement vectors of the linear elastic cantilever beam problem, respectively. It can be seen that some accurate results for the displacements and the stresses are obtained by using the ORCM.

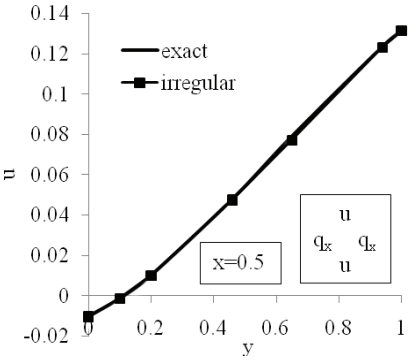

Figure 15: Values of u at x=0.5 by irregular nodal model of 89 nodes, for the second mixed problem of Poisson's equation

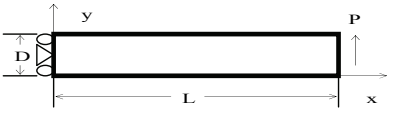

Figure 16: The linear elastic cantilever beam with a parabolic-shear end load

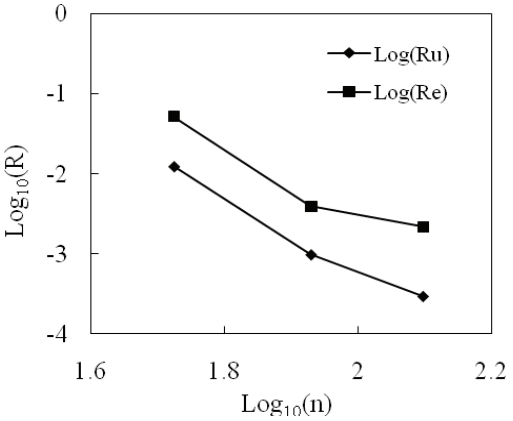

Figure 17: Relative errors and convergences for the linear elastic cantilever beam problem (n is number of the nodes)

7 Conclusions

In this paper, the ORCM is proposed. By introducing some collocation points, which are located at outside of domain of the analyzed body, unsatisfactory issue of the positivity conditions of boundary points in collocation methods can be avoided. Convergence studies in the numerical examples show that the ORCM possesses good convergence for both the unknown variables and their derivatives. Poisson's

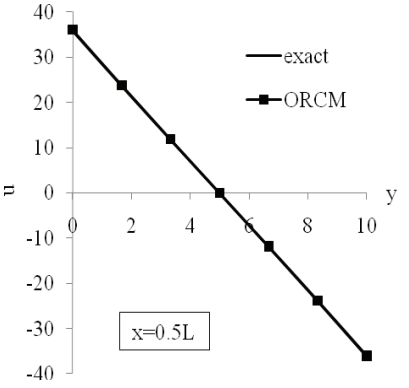

Figure 18: Values of u at x=0.5L by regular nodal model of 125 nodes, for the linear elastic cantilever beam problem

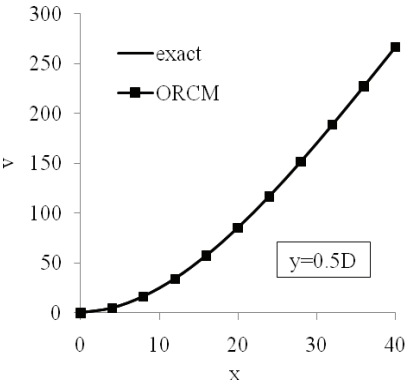

Figure 19: Values of v at y=0.5D by regular nodal model of 125 nodes, for the linear elastic cantilever beam problem

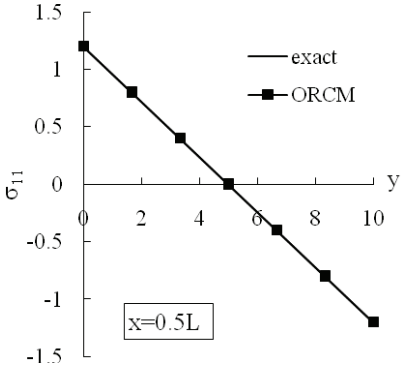

Figure 20: Values of σ_{11} at x=0.5L by regular nodal model of 125 nodes, for the linear elastic cantilever beam problem

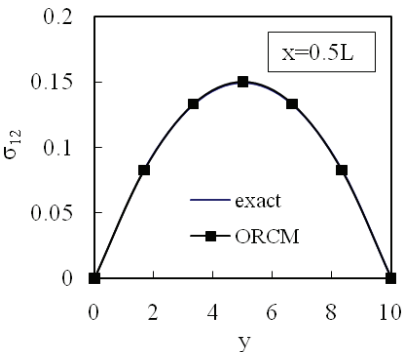

Figure 21: Values of σ_{12} at x=0.5L by regular nodal model of 125 nodes, for the linear elastic cantilever beam problem

problem and the linear elastic cantilever beam problem are analyzed by using the ORCM, and quite accurate numerical results have been obtained. The ORCM does not demand any specific kind of partial differential equations, therefore it shows promise of wide engineering applications of the ORCM. The directions of future investigations on the ORCM will be solving problems of nonlinear partial differential equations and metal forming.

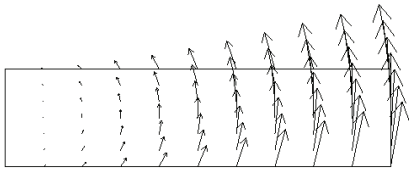

Figure 22: Numerical displacement vectors of the linear elastic cantilever beam problem by ORCM with regular nodal model of 125 nodes

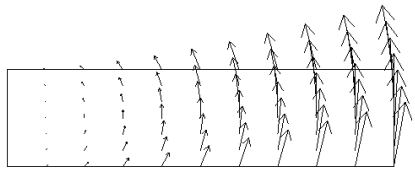

Figure 23: Exact displacement vectors of the linear elastic cantilever beam problem at the same points with Fig. 22

References

Aluru, N. R. (2000): A point collocation method based on reproducing kernel approximations. *Int. J. Numer. Methods Engrg.*, vol. 47, pp. 1083-1121.

Atluri, S. N.; Zhu, T. (1998): A new meshless local Petrov-Galerkin (MLPG) approach in computational mechanics. *Computational Mechanics*, vol.22, pp. 117-127.

Atluri, S. N.; Kim, H. G.; Cho, J.Y. (1999): A critical assessment of the truly meshless local Petrov-Galerkin (MLPG), and local boundary integral equation (LBIE) methods. *Computational Mechanics*, vol. 24, pp. 348-372.

Atluri, S. N.; Liu, H. T.; Han, Z. D. (2006a): Meshless local Petrov-Galerkin (MPLG) mixed collocation method for elasticity problems. *CMES: Computer Modeling in Engineering & Sciences*, vol. 14, pp. 141-152.

Atluri, S. N.; Liu, H. T.; Han, Z. D. (2006b): Meshless local Petrov-Galerkin (MPLG) mixed finite difference method for solid mechanics. *CMES: Computer Modeling in Engineering & Sciences*, vol. 15, pp. 1-16.

Belytschko, T.; Lu, Y. Y.; Gu, L. (1994): Element free Galerkin methods. *Int. J. Numer. Methods Engrg.*, vol. 37, pp. 229-256.

Boroomand, B.; Tabatabaei, A. A.; Onate, E. (2005): Simple modifications for stabilization of the finite point method. *Int. J. Numer. Methods Engrg.*, vol. 63, pp. 351-379.

Chantasiriwan, S. (2006): Performance of multiquadric collocation method in solving lid-driven cavity flow problem with low Reynolds number. *CMES: Computer Modeling in Engineering & Sciences*, vol. 15, pp. 137-146.

Demkowicz, L.; Karafilt, A.; Liszka, T. (1984): On some convergence results for FDM with irregular mesh. *Comput. Methods Appl. Mech. Engrg.*, vol. 42, pp. 343-355.

Duarte, C. A.; Oden, J. T. (1996): An h-p adaptive method using clouds. *Comput. Methods Appl. Mech. Engrg.*, vol. 139, pp. 237-262.

Guo, Y.-M. (2009): A metal forming analysis by using the hybrid PCM/FEM. *CMES: Computer Modeling in Engineering & Sciences*, vol. 41, pp. 177-193.

Jin, X.; Li, G.; Aluru, N. R. (2004): Positivity conditions in meshless collocation methods. *Comput. Methods Appl. Mech. Engrg.*, vol. 193, pp. 1171-1202.

Kosec, G.; Sarler, B. (2008): Local RBF collocation method for Darcy flow. *CMES: Computer Modeling in Engineering & Sciences*, vol. 25, pp. 197-207.

Li, Shu; Atluri, S. N. (2008a): Topology-optimization of structures based on the MPLG mixed collocation method. *CMES: Computer Modeling in Engineering & Sciences*, vol. 26, pp. 61-74.

Li, Shu; Atluri, S. N. (2008b): The MPLG mixed collocation method for material orientation and topology optimization of anisotropic solids and structures. *CMES: Computer Modeling in Engineering & Sciences*, vol. 30, pp. 37-56.

Liu, W. K.; Jun, S.; Li, S.; Adee, J.; Belytschko, T. (1995): Reproducing kernel particle methods for structural dynamics. *Int. J. Numer. Methods Engrg.*, vol. 38, pp. 1655-1679.

Melenk, J. M.; Babuska, I. (1996): The partition of unity finite element method: basic theory and applications. *Comput. Methods Appl. Mech. Engrg.*, vol. 139, pp. 289-314.

Nayroles, B.; Touzot, G.; Villon, **P.** (1992): Generalizing the FEM: diffuse approximation and diffuse elements. *Computational Mechanics*, vol. 10, pp. 307-318.

Onate, E.; Idelsohn, S.; Zienkiewicz, O. C.; Toylor, R. L. (1996a): A finite point method in computational mechanics. Applications to convective transport and fluid flow. *Int. J. Numer. Methods Engrg.*, vol. 39, pp. 3839-3866.

Onate, E.; Idelsohn, S.; Zienkiewicz, O. C.; Toylor, R. L.; **Sacco, C.** (1996b): A stabilized finite point method for analysis of fluid mechanics problems. *Comput. Methods Appl. Mech. Engrg.*, vol. 139, pp. 315-346.

Patanakar, S. V. (1980): *Numerical Heat Transfer and Fluid Flow*, Hemisphere.

Wen, P. H.; Hon, Y. C. (2007): Geometrically nonlinear analysis of Reissner-Mindlin Plate by meshless computation. *CMES: Computer Modeling in Engineering & Sciences*, vol. 21, pp. 177-191.

Wu, C.-P.; Chiu, K.-H.; Wang, Y.-M. (2008): A mesh-free DRK-based collocation method for the coupled analysis of functionally graded magneto-electro-elastic shells and plates. *CMES: Computer Modeling in Engineering & Sciences*, vol. 35, pp. 181-214.

Wu, X.-H.; Shen, S.-P.; Tao, W.-Q. (2007): Meshless local Petrov-Galerkin collocation method for two-dimensional heat conduction problems. *CMES: Computer Modeling in Engineering & Sciences*, vol. 22, pp. 65-76.

Yang, C.; Tang, D.; Yuan, C.; Kerwin, W.; Liu, F.; Canton, G.; Hatsukami, T. S.; Atluri, S. N. (2008): Meshless generalized finite difference method and human carotid atherosclerotic plaque progression simulation using multi-year MRI patient-tracking data. *CMES: Computer Modeling in Engineering & Sciences*, vol. 28, pp. 95-107.

Zhu, T.; Zhang, J.; Atluri, S. N. (1998): A local boundary integral equation (LBIE) method in computational mechanics and a meshless discretization approach. *Computational Mechanics*, vol.21, pp. 223-235.